Title

Evolution and mechanics of mixed phospholipid fibrinogen monolayers

Journal

Journal of The Royal Society Interface, 15(141)

ISSN

1742-5689

Authors

Williams, Ian

Squires, Todd M

Publication Date

2018-04-01

DOI

10.1098/rsif.2017.0895

Peer reviewed

INTERFACE

rsif.royalsocietypublishing.org

Research

Cite this article: Williams I, Squires TM. 2018 Evolution and mechanics of mixed phospholipid fibrinogen monolayers. *J. R. Soc. Interface* **15**: 20170895.
http://dx.doi.org/10.1098/rsif.2017.0895

Received: 30 November 2017
Accepted: 9 March 2018

Subject Category:
Life Sciences–Physics interface

Subject Areas:
biophysics

Keywords:
monolayers, lung surfactant, fibrinogen, interfacial rheology, protein adsorption

Author for correspondence:
Ian Williams
e-mail: ian.williams@engineering.ucsb.edu

Electronic supplementary material is available online at https://dx.doi.org/10.6084/m9.figshare.c.4035092.

THE ROYAL SOCIETY PUBLISHING

Evolution and mechanics of mixed phospholipid fibrinogen monolayers

Ian Williams and Todd M. Squires

Department of Chemical Engineering, University of California, Santa Barbara, CA, USA

IW, 0000-0001-6997-1823

All mammals depend on lung surfactant (LS) to reduce surface tension at the alveolar interface and facilitate respiration. The inactivation of LS in acute respiratory distress syndrome (ARDS) is generally accompanied by elevated levels of fibrinogen and other blood plasma proteins in the alveolar space. Motivated by the mechanical role fibrinogen may play in LS inactivation, we measure the interfacial rheology of mixed monolayers of fibrinogen and dipalmitoylphosphatidylcholine (DPPC), the main constituent of LS, and compare these to the single species monolayers. We find DPPC to be ineffective at displacing preadsorbed fibrinogen, which gives the resulting mixed monolayer a strongly elastic shear response. By contrast, how effectively a pre-existing DPPC monolayer prevents fibrinogen adsorption depends upon its surface pressure. At low DPPC surface pressures, fibrinogen penetrates DPPC monolayers, imparting a mixed viscoelastic shear response. At higher initial DPPC surface pressures, this response becomes increasingly viscous-dominated, and the monolayer retains a more fluid, DPPC-like character. Fluorescence microscopy reveals that the mixed monolayers exhibit qualitatively different morphologies. Fibrinogen has a strong, albeit preparation-dependent, mechanical effect on phospholipid monolayers, which may contribute to LS inactivation and disorders such as ARDS.

1. Introduction

The primary purpose of the lung is to exchange gas across a complex aqueous–air interface [1]. This is facilitated by an interfacial area of up to approximately 70 m^2 in human adults [2–5]. Upon inhalation, alveoli are inflated, creating surface area and performing work against the surface tension, γ, potentially consuming substantial metabolic energy. An adsorbed multicomponent layer of lipids and proteins, collectively known as lung surfactant (LS), reduces γ significantly [1,2,6–8], lowering the energetic cost of inhalation, preventing alveolar collapse during exhalation and stabilizing small airways [9].

Inactivation of LS causes breathing difficulties and serious respiratory disorders including acute respiratory distress syndrome (ARDS), in which γ cannot be sufficiently reduced, decreasing lung compliance and increasing the energetic cost of breathing [8,10]. Dire consequences of inactivated LS include: alveolar collapse (atelectasis), reduction in functional residual capacity (the lung volume remaining after exhalation), pulmonary bleeding and systemic oxygen starvation [2,4,8–12]. ARDS develops rapidly, typically within 24 h of an identifiable lung trauma [2,8], and is fatal in approximately 30–40% of patients [13]. No treatment has proved generally successful.

Many factors may contribute to LS inactivation [14] and the onset and progression of ARDS. The lungs of ARDS patients often contain water-soluble surface active materials that are not present in healthy alveoli. Bile salts, lysolipids, serum proteins, meconium, different lipids and fatty acids and air pollutants are all thought to inhibit the ability of LS to reduce γ [1,2] and are found at elevated levels in the bronchoalveolar lavage (BAL) fluid extracted from ARDS patients [15–17]. In particular, surface adsorption of blood proteins including fibrinogen [18–20], albumin [15,18,21] and haemoglobin [22] is associated with LS inactivation [9,16,23]. However, mechanism(s) by which

these proteins inhibit LS function, or how to reverse these effects, are far from understood [8]. In fact, it is not known whether the presence of serum proteins in the BAL fluid is simply a passive symptom that correlates with ARDS, or whether serum proteins play an active role in its progression.

Informed and inspired by these observations, we present a physico-chemical study of fibrinogen, which is believed to inhibit LS function more severely than other blood proteins [18,20], characterizing its effect on a model phospholipid monolayer under idealized, laboratory conditions. Fibrinogen adsorbs at an aqueous–air interface, forming a monolayer of molecules which become increasingly aligned with increasing surface density [24–27], and therefore may compete with LS to adsorb in the alveoli, potentially promoting inactivation. Thus, it is important to understand fibrinogen's effect on surface tension, and how it alters the structural and rheological properties of phospholipid monolayers. As a proxy for LS, which is a multicomponent mixture of lipids and proteins, we use the most abundant LS molecule, dipalmitoylphosphatidylcholine (DPPC) [1]. We first characterize the adsorption of fibrinogen at an aqueous–air interface. Subsequently, we probe the effect of fibrinogen on the rheological response of DPPC monolayers using a unique interfacial rheometry technique [28]. We describe two distinct 'orders of operations': DPPC spread onto pre-adsorbed fibrinogen monolayers, and fibrinogen introduced to the subphase under pre-formed DPPC monolayers. Distinct behaviours are observed in these two cases. Additionally, fluorescence microscopy allows direct visualization of monolayer morphology so that rheological changes can be related to changes in mesostructure as fibrinogen adsorbs. Finally, we discuss the ways in which our simplified laboratory studies may relate to the action of real LS at physiological conditions, and expected differences.

2. Experimental details

The aqueous phase in all experiments is phosphate-buffered saline (PBS, Sigma Aldrich), containing 0.01 M phosphate buffer, 0.0027 M potassium chloride and 0.137 M sodium chloride. DPPC is obtained in chloroform from Avanti Polar Lipids and diluted with HPLC grade chloroform (Sigma-Aldrich) to yield solutions with concentrations in the range 0.1–1 mg ml^{-1}. To provide fluorescence contrast [29,30], DPPC samples are doped with 0.5 wt% Texas Red DHPE (Texas Red 1,2-dihexadecanoyl-*sn*-glycero-3-phosphoethanolamine) supplied by Life Technologies. Fibrinogen from bovine plasma (Sigma-Aldrich) is purchased as a powder and dissolved in PBS.

Experiments employ a custom Teflon Langmuir trough and a bright-field/fluorescence microscope. Microrheological measurements are made in bright-field mode using a 10 × magnification Nikon Plan Fluor objective. Monolayer morphology is visualized in fluorescence mode using a Nikon L Plan super long working distance 50 × magnification objective. The Langmuir trough has two reservoirs separated by a central observation area (figure 1*a*). A pair of computer-controlled Teflon barriers allow compression of the interface. Surface pressure ($\Pi = \gamma_0 - \gamma$, the reduction in γ compared to the clean interface) is monitored using a filter paper Wilhelmy tensiometer (Riegler and Kirstein, Germany). Unless otherwise noted, the trough is cleaned before every

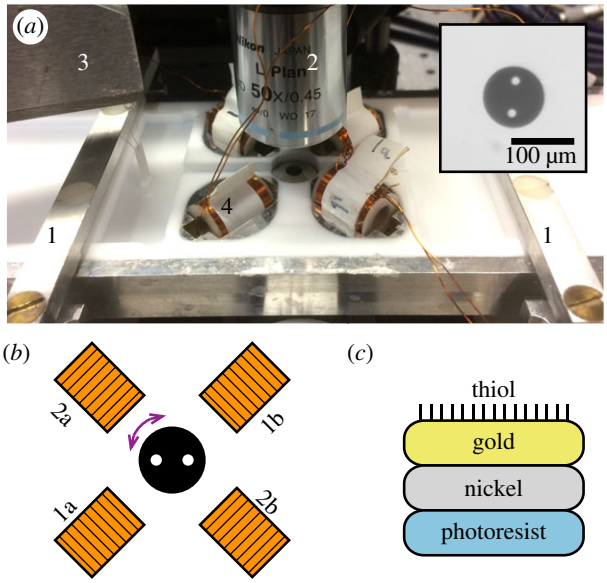

Figure 1. (*a*) Photograph of apparatus. A Langmuir trough with two movable barriers (1) is observed through a microscope objective (2). A filter paper Wilhelmy tensiometer (3) monitors surface pressure. Electromagnets (4) apply magnetic fields at the observation region. Inset shows micrograph of microbutton. (*b*) Schematic of electromagnet array and microbutton probe. Magnets 1a and 1b are connected in series and used to apply an oscillating magnetic field. Magnets 2a and 2b are connected independently and used to translate or align the probe. (*c*) Side-view schematic of microbutton. A ferromagnetic nickel layer is deposited onto SU-8 photoresist. Gold provides an anchoring point for a thiol monolayer, giving an amphiphilic character.

experiment by wiping all surfaces with methanol and rinsing three times each with acetone, isopropyl alcohol and deionized water (Milli-Q). All experiments are performed at room temperature, 20°C.

The magnetic microbutton interfacial microrheometry technique has been described at length elsewhere [28,31–33]. A photolithographically fabricated, amphiphilic, ferromagnetic probe of radius $a = 50$ µm (figure 1) is deposited on the interface at the centre of an array of four electromagnets. Passing a sinusoidal current through a pair of oppositely aligned magnets (1a and 1b in figure 1*b*) connected in series creates a sinusoidal magnetic field at the trough centre. By virtue of its nickel layer (figure 1*c*), the microbutton responds to align its magnetic moment with the field. The perpendicularly aligned magnets (2a and 2b) are controlled independently to align or translate the probe.

The probe's 'buttonholes' are tracked to measure its angular response to the applied field. Interfacial mechanical properties are inferred by interpreting this response. The microbutton is aligned perpendicularly to the field such that the magnitude of the applied torque is $\Gamma \approx mB$ where m and B are the magnitudes of the probe magnetic moment and the magnetic field, respectively.

An oscillating magnetic field, $B_0\,e^{i\omega t}$, applies an oscillatory torque to the probe,

$$\Gamma_0\,e^{i\omega t} = mB_0\,e^{i\omega t}, \tag{2.1}$$

which drives an angular response:

$$\theta(t) = \theta_0\,e^{i(\omega t-\delta)}, \tag{2.2}$$

where θ_0 is the amplitude of probe oscillation and δ represents a phase lag with respect to the torque. The complex

rotational resistance

$$\zeta_R^*(\omega) = \frac{mB_0\, e^{i\delta}}{i\omega\theta_0} \tag{2.3}$$

relates the torque and angular velocity. Both subphase fluid viscosity, η, and interfacial viscosity, η_S, contribute to ζ_R^*. The Boussinesq number,

$$B_0 = \frac{\eta_S}{\eta a} \tag{2.4}$$

characterizes the relative magnitude of the drag on the probe due to the surface and the subphase. In the limit $B_0 \gg 1$, interfacial drag dominates, and the rotational resistance is given by $\zeta_R = 4\pi\eta_S a^2$ [33,34]. In this limit, the complex surface viscosity, η_S^*, is

$$\eta_S^*(\omega) = \frac{mB_0\, e^{i\delta}}{i\omega\theta_0 4\pi a^2}. \tag{2.5}$$

This is related to the linear viscoelastic surface moduli, $G_S^*(\omega) = G_S'(\omega) + iG_S''(\omega)$ by $G_S^*(\omega) = i\omega\eta_S^*(\omega)$. The interfacial storage modulus, G_S', characterizing the elastic response, is given by the in-phase motion of the microbutton, while the interfacial loss modulus, G_S'', which characterizes viscous behaviour, is given by its out-of-phase response [33,35,36]. Practically, B_0 and θ_0 are obtained from sinusoidal fits to the recorded magnetic field and microbutton orientation and δ is the phase lag between these sinusoids.

For experiments without fibrinogen, or where fibrinogen is introduced during the experiment, m is measured prior to introducing any surface active material. On a clean buffer–air interface, the probe experiences the subphase drag dominated, low-Bo regime, in which rotational resistance is $\zeta_R = 16\eta a^3/3$ [33,34] and the real part of (2.3) gives

$$m = \frac{16\eta a^3 \omega\theta_0}{3B_0 \sin\delta}. \tag{2.6}$$

Using η for PBS, m is measured by observing a disc's response to an oscillating field of known amplitude and frequency [31]. For each probe, m is taken to be the average of at least 30 measurements. Individual microbuttons cannot be calibrated this way with fibrinogen solution subphases, in which case analysis is performed using the average value $\bar{m} = 203 \times 10^{-17}\,\mathrm{J\,G^{-1}}$, obtained from calibrations of 50 different probes.

Following microbutton calibration, DPPC is spread on the interface and/or fibrinogen is injected into the subphase. DPPC is spread from chloroform solution using a microsyringe. After spreading, 30 min are allowed to ensure the chloroform evaporates. The trough barriers compress the interface at a rate of $0.8\,\mathrm{cm^2\,s^{-1}}$ when compression is required. B_0 is manually adjusted to maintain small probe oscillations of $\lesssim 0.05$ radians. An upper limit to the measurable surface moduli is set for any given m by the maximum B_0 that can be applied. All oscillatory microrheological measurements are performed at 1 Hz. The shear response of a material is, in general, dependent on the rate at which it is deformed. However, due to the dynamic, non-equilibrium nature of our adsorption and penetration experiments, it is not possible to perform full frequency sweeps during monolayer evolution. A frequency of 1 Hz is chosen for its relevance to the timescales of breathing, to allow comparison with the existing literature [32,37], and to track the temporal evolution of ageing monolayers.

3. Results and discussion

3.1. Fibrinogen adsorption

While fibrinogen is known to adsorb at the aqueous–air interface [24–26,38,39], little attention has been paid to its interfacial shear rheology, either in equilibrium or during adsorption. Using a macroscopic rheometer, Ariola *et al.* [37] measured steady-state interfacial moduli as a function of bulk concentration, c. Below an onset concentration, there is no measurable interfacial rheology. Above this concentration, the response is viscous-dominated with $G_S'' > G_S'$. Both $G_S'(c)$ and $G_S''(c)$ exhibit a peak at $c \approx 0.1\,\mathrm{mg\,ml^{-1}}$.

We first characterize fibrinogen adsorption by monitoring $\Pi(t)$. Because fibrinogen adsorbs at both the aqueous–air interface and Teflon surfaces [40], two series of experiments are performed. In the first series, the standard trough cleaning procedure is followed. To assess the impact of adsorption at the trough walls, the second series is performed without cleaning between measurements, instead only rinsing with DI water. As such, the trough is pretreated with fibrinogen.

Typical clean trough data are presented in figure 2*a* for subphase concentrations $0.0002\,\mathrm{mg\,ml^{-1}} \leq c \leq 1\,\mathrm{mg\,ml^{-1}}$. Experiments in pretreated troughs exhibit qualitatively identical behaviour (see the electronic supplementary material). Below an onset concentration at $c \approx 0.003\,\mathrm{mg\,ml^{-1}}$, surface pressure remains unmeasurably small over a timescale of hours. Above this concentration, Π increases after a concentration-dependent induction time, and eventually approaches a plateau at steady state.

These data follow asymmetric sigmoidal curves, approaching their plateaux more slowly than they rise from $\Pi = 0$, and are fit with an empirical function of the form

$$\Pi(t) = \Pi_0 \exp\left[-a\exp\left(-bt\right)\right], \tag{3.1}$$

which captures their shape. Three parameters are extracted from these fits. The spreading pressure is given by the long time plateau, Π_0. The time at the point of inflection, $t^* = b^{-1}\ln a$, gives an adsorption timescale, and the gradient at t^*, $\dot{\Pi}(t^*) = \Pi_0 b e^{-1}$, quantifies the rate of adsorption. The dependence of these parameters on c is shown in figure 2*b–d* for both clean (circles) and pretreated (triangles) troughs.

Figure 2*b* reveals that the spreading pressure is immeasurably small ($\Pi_0 \approx 0$) below the onset concentration. This jumps to $\Pi_0 \approx 8\,\mathrm{mN\,m^{-1}}$ just above the onset concentration, then increases to $\Pi_0 \approx 15\,\mathrm{mN\,m^{-1}}$ over nearly three decades in concentration, consistent with similar experiments in the literature [37]. Π_0 measured in clean and pretreated troughs agree quantitatively, except very close to the onset concentration.

Figure 2*c*,*d* shows that the adsorption timescale, t^*, decreases sharply as c is increased, while the adsorption rate increases, as is typical for protein adsorption [41,42]. At high concentrations ($c \gtrsim 0.1\,\mathrm{mg\,ml^{-1}}$), fibrinogen adsorbs so quickly that the inflection point in the fitted curve appears to occur at negative times. This region is indicated with red shading. In pretreated troughs at nominally identical subphase concentrations, adsorption timescales decrease slightly and adsorption rates increase slightly. Differences between pretreated and clean experiments remain very small, except very close to the onset concentration. In experiments combining fibrinogen and DPPC, precise knowledge

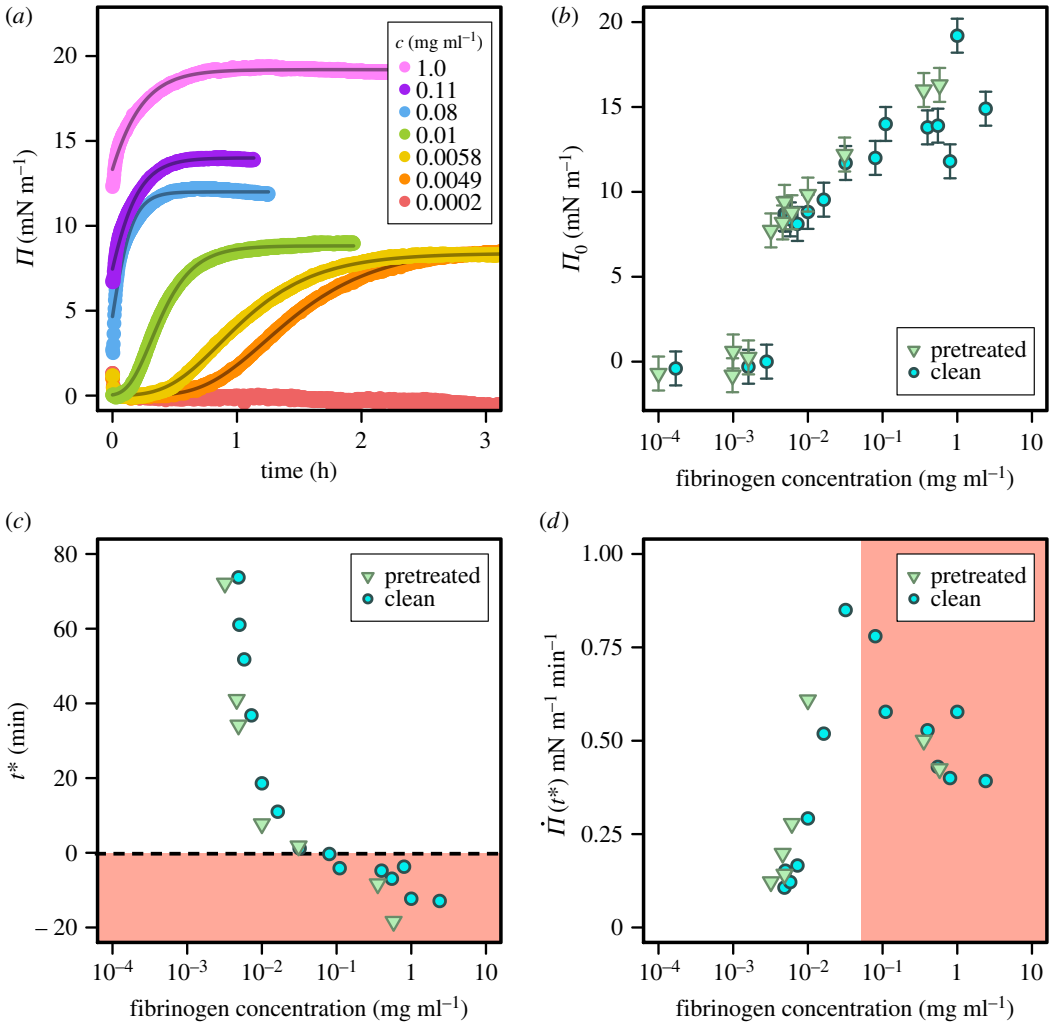

Figure 2. (*a*) $\Pi(t)$ during fibrinogen adsorption at a range of subphase fibrinogen concentrations, c. Lines show fits described in text. (*b*) Spreading pressure, (*c*) adsorption timescale and (*d*) adsorption rate as a function of c in clean (circles) and pretreated (triangles) trough. Red shaded region in (*c*) and (*d*) represents high c data for which $t^* < 0$.

of c is of lesser importance than strict trough hygiene, and thus we neglect fibrinogen adsorption to the walls (further exploration of this effect is included in the electronic supplementary material).

Figure 3*a*,*b* shows the evolution of G'_S and G''_S as monolayers adsorb from solutions at various concentrations, c. Surface rheology evolves like $\Pi(t)$ in figure 2. No change in G'_S or G''_S is measured when $c \lesssim 0.003\,\mathrm{mg\,ml^{-1}}$, which coincides with the onset concentration for measurable Π. Interfacial stiffening occurs so rapidly at high concentrations ($c \gtrsim 0.01\,\mathrm{mg\,ml^{-1}}$) that the probe cannot be reliably torqued to obtain meaningful measurements. In the intermediate regime, the interfacial response is initially viscous-dominated ($G''_S > G'_S$) but G'_S ultimately overtakes G''_S, indicating a crossover to elastic-dominated behaviour. The moduli increase beyond the upper limit of measurability in all experiments above the onset concentration. Therefore, the plateaux observed in figure 3 do not represent equilibrium values of G'_S and G''_S. Clearly, however, fibrinogen forms very stiff, elastic monolayers, with increasing rapidity as c is increased.

Π continues to grow after the monolayer becomes so stiff that the probe no longer responds to maximum torque, indicating that fibrinogen continues to adsorb (figure 3*c*). In all experiments, G'_S increases by three orders of magnitude before Π increases measurably above approximately 0 mN $\mathrm{m^{-1}}$, showing that fibrinogen influences interfacial rheology at surface concentrations much lower than those required to modify γ. A very small amount of fibrinogen adsorbed to an aqueous–air interface has a very large impact on its material properties. This is a significant observation, indicating that microrheometry may be more sensitive to adsorbed material than surface pressure measurements.

3.2. Dipalmitoylphosphatidylcholine phase behaviour and interfacial rheology

The monolayer rheology and phase behaviour of DPPC are well established [32,43–45]. Figure 4*a* shows the pressure-area isotherm of a DPPC monolayer (black circles) encoding its phase behaviour. At low molecular density (high area per molecule), DPPC exists in a liquid expanded (LE) state, in which head groups are translationally disordered and tails are orientationally disordered. LE DPPC can incorporate the fluorescently labelled DHPE, and appears bright in fluorescence micrographs (inset to figure 4*a*). Upon compression, the surface pressure increases until a plateau is reached, representing coexistence between liquid expanded and liquid condensed (LC) DPPC. The surface pressure of LE–LC coexistence increases with temperature [44,46–48], but its onset occurs at approximately 4 mN $\mathrm{m^{-1}}$ at 20°C. In this region domains of LC DPPC nucleate and grow, until the entire monolayer is in the LC state at $\Pi \approx 10\,\mathrm{mN\,m^{-1}}$.

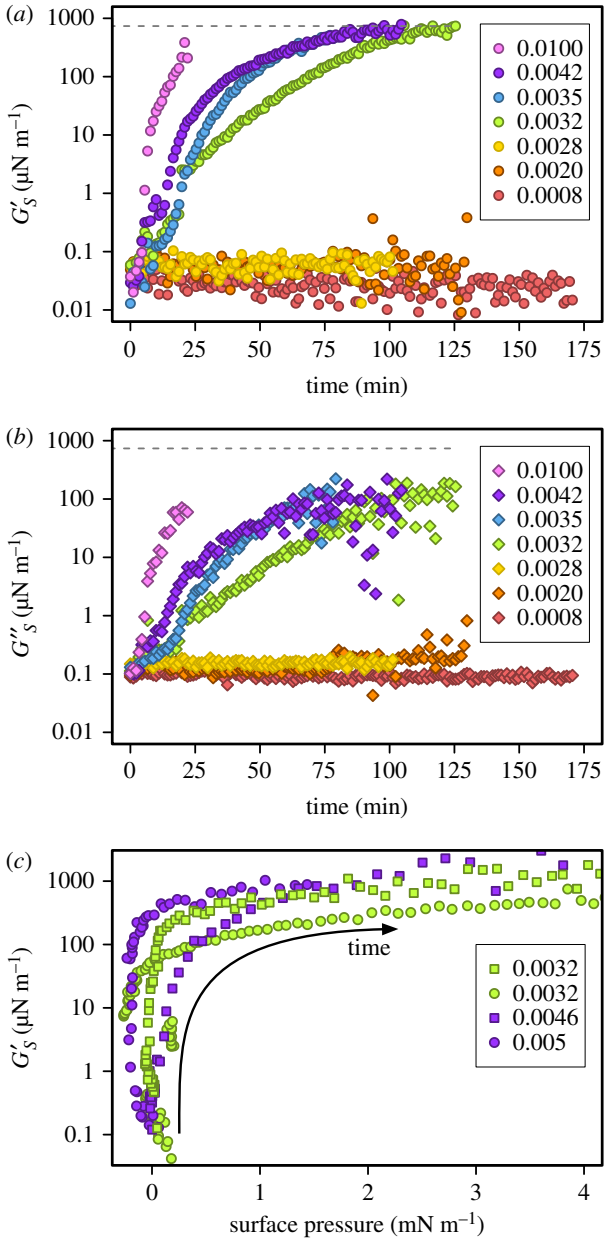

Figure 3. Surface shear moduli (*a*) $G'_S(t)$ and (*b*) $G''_S(t)$ of fibrinogen adsorbing from solution in clean trough at c indicated in legend. Dashed line indicates maximum measurable modulus assuming $m = 203 \times 10^{-17}$ J G^{-1}. (*c*) $G'_S(\Pi)$ during fibrinogen adsorption from solutions at c indicated in legend. Time proceeds in direction of arrow. Experiments performed in clean (circles) and pretreated (squares) troughs. Concentrations in mg ml^{-1}.

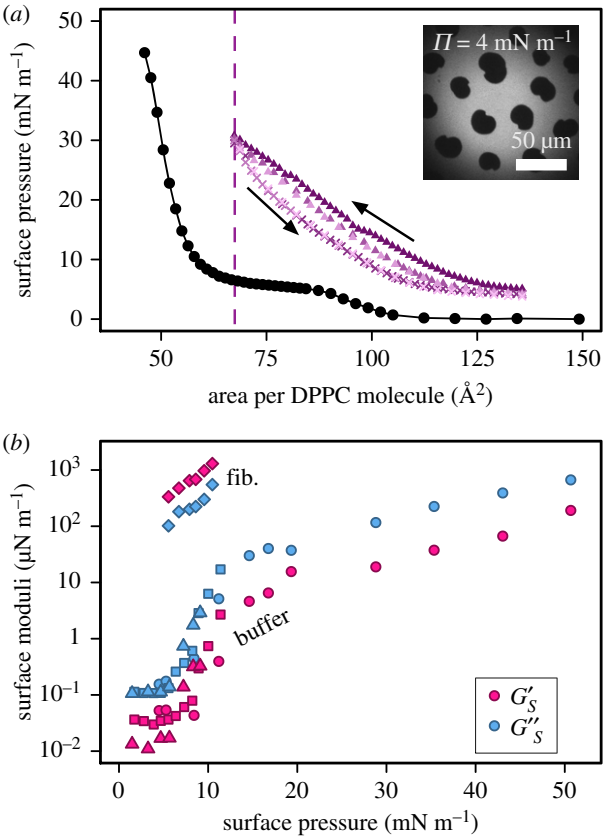

Figure 4. (*a*) Pressure–area isotherms of DPPC on PBS (black circles) and on a subphase containing 0.0011 mg ml^{-1} fibrinogen (pink triangles and crosses). Solid symbols: compression; crosses: decompression. Dashed line indicates collapse of mixed monolayer. Inset: micrograph of DPPC monolayer at $\Pi = 4$ mN m^{-1} showing LC domains. (*b*) $G'_S(\Pi)$ and $G''_S(\Pi)$ for DPPC on PBS (circles, triangles and squares) and on a subphase containing 0.0012 mg ml^{-1} fibrinogen (diamonds). Symbol shape represents independent experiments and each symbol is the average of at least 10 measurements.

The molecules in LC domains are regularly packed and exclude the fluorophore, thus appearing dark in fluorescence micrographs.

The Π-dependent interfacial rheology of DPPC monolayers has been measured on room temperature DI water subphases using magnetic microbutton microrheometry [32]. Figure 4*b* shows new measurements made on PBS that exhibit the same qualitative features. Starting at $\Pi \approx 5$ mN m^{-1}, DPPC has a measurable effect on interfacial rheology with both G'_S and G''_S rising exponentially with Π. This sharp growth coincides with LE–LC coexistence. It has been hypothesized that the moduli increase as a power law in the area fraction of LC domains [49]. Beyond coexistence, $\Pi \gtrsim 10$ mN m^{-1}, both G'_S and G''_S exhibit weaker exponential growth. The entire monolayer is condensed, and further increasing Π causes a smaller increase in G'_S and G''_S. The shear response of the DPPC monolayer is viscous-dominated ($G''_S > G'_S$) at all Π.

3.3. Mixing protocol I: dipalmitoylphosphatidylcholine added to fibrinogen monolayer

In the first mixing scenario, the trough is filled with a fibrinogen solution which is allowed to adsorb at the interface, then DPPC is spread on top so that it interacts with a pre-adsorbed fibrinogen layer. The subphase concentration is $c \approx 0.001$ mg ml^{-1}, below the onset concentration, and so no rise in Π or the interfacial moduli is measured before spreading DPPC. The fibrinogen solution is left to equilibrate for at least 3 h before the DPPC is spread, and a further 30 min are allowed for chloroform evaporation, monolayer mixing and equilibration. The monolayer is then compressed and the surface moduli are measured as a function of Π.

Immediately following spreading DPPC, Π jumps to around 4 mN m^{-1}. Accompanying this rapid Π increase is an equally sudden interfacial stiffening. A probe that easily oscillates on the fibrinogen subphase becomes immobile following the addition of DPPC and requires a large increase in B_0 to restore measurable oscillation. Figure 4*a* shows how the pressure–area isotherm of DPPC is modified when it is spread onto a preadsorbed fibrinogen monolayer. Compression isotherms are shown as solid triangles and crosses represent decompression. The darkest triangles show the

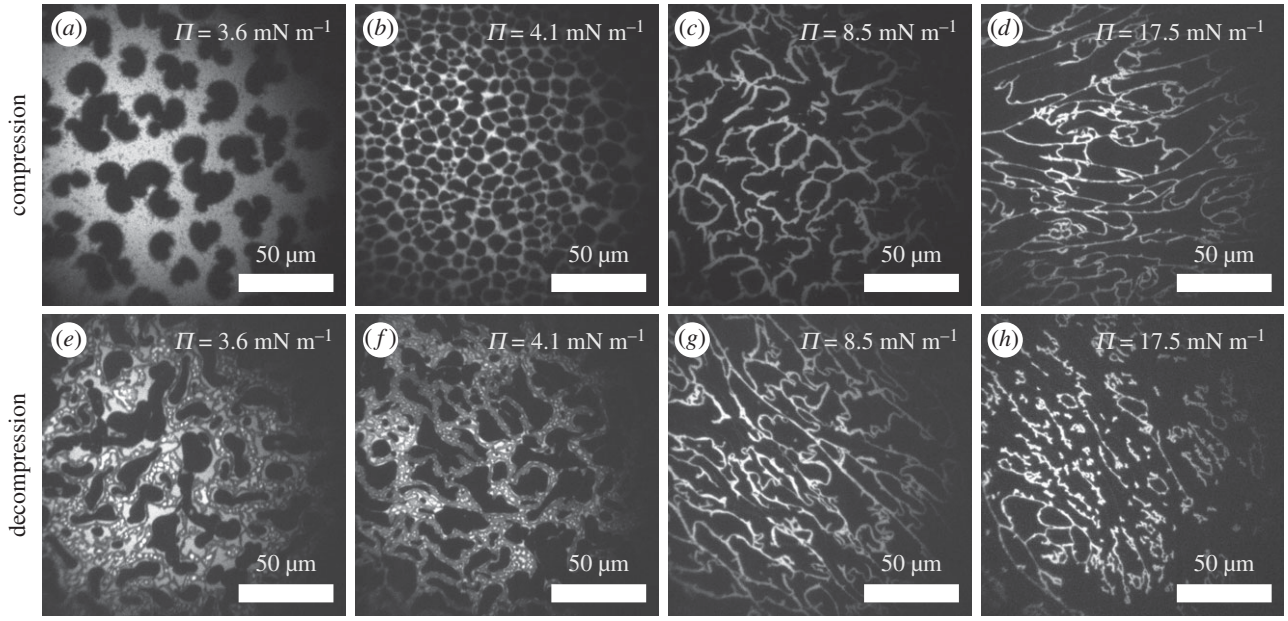

Figure 5. Fluorescence micrographs showing morphology of DPPC spread onto fibrinogen preadsorbed from a subphase containing 0.0011 mg ml^{-1} at comparable Π during compression (*a–d*) and decompression (*e–h*). Scale bars are 50 µm.

first compression, and subsequent decompression–recompression cycles are shown in progressively lighter shades. At any given interfacial area, Π is significantly higher for these mixed monolayers than would be measured for either DPPC or fibrinogen alone, indicating the presence of both DPPC and fibrinogen in the monolayer. The Π jump on spreading puts DPPC into its coexistence plateau. On compression, Π increases up to approximately 30 mN m^{-1}, beyond which point monolayers start to collapse. Decompression measurements fall below the compression isotherms, showing reproducible hysteresis characteristic of slow respreading [50]. While all three decompression curves fall on top of one another, only the second and third compressions follow the same curve, with the initial compression offset at higher Π. This suggests either that adsorbed material is ejected during the first compression and not readsorbed [50] or that the first compression causes some structural change or complexation that is not reversed on decompression. The identical second and third compression isotherms suggest no further change in composition or structure occurs in subsequent cycles.

The interfacial rheology of DPPC spread onto preadsorbed fibrinogen is shown as diamonds in figure 4*b*. The mixed monolayer exhibits an increase in G'_S of nearly five orders of magnitude, and an increase in G''_S of at least two orders of magnitude over pure DPPC. Furthermore, the mixed monolayer shows elastic-dominated behaviour ($G'_S > G''_S$) whereas DPPC alone exhibits a primarily viscous response ($G''_S > G'_S$). Even at very low surface concentration, pre-existing fibrinogen monolayers stiffen DPPC dramatically. In fact, by $\Pi \approx 12$ mN m^{-1}, the mixed monolayer becomes immeasurably stiff, while G'_S and G''_S in the pure DPPC monolayer remain measurable up to significantly higher Π.

Fluorescence imaging of the mixed monolayer during compression and decompression reveals considerable changes in its morphology when compared with pure DPPC. Figure 5*a* shows the initial state of the monolayer after spreading DPPC, but before compression. The dark domains are reminiscent of LC regions in the pure DPPC monolayer at coexistence (inset to figure 4*a*), but the bright, disordered regions contain small, dark microdomains not seen in LE DPPC. Compressing the interface squeezes these domains together, forming the bright network structure shown in figure 5*b*. By $\Pi = 5$ mN m^{-1}, the mixed monolayer consists of irregular dark regions separated by a bright network. This structure persists up to $\Pi \approx 20$ mN m^{-1} where fluorescence is quenched, potentially due to fluorophore crowding [51].

On decompression, the network initially breaks (figure 5*h*), but reforms and persists down to $\Pi \approx 6$ mN m^{-1}. Around $\Pi =$ 5 mN m^{-1}, the network arms thicken, introducing spotted textures of varying brightness (figure 5*e*,*f*). Each discrete intensity level presumably contains different compositions of LC DPPC, LE DPPC, DHPE and fibrinogen. This new structure persists for at least 24 h, and does not relax to the morphology of figure 5*a*, suggesting irreversible changes or kinetically trapped states are introduced through compression and decompression. Subsequent recompression–decompression cycles recover the irregular network at high Π, and the multiple-intensity morphologies at low Π (electronic supplementary material). This suggests that complexation during compression is responsible for the offset of the first compression isotherm from subsequent recompressions.

One conclusion to draw is that DPPC is not effective at removing fibrinogen that has already adsorbed to aqueous–air interfaces, even when fibrinogen is so dilute that it has no measurable effect on Π or interfacial rheology. This draws an intriguing contrast with previous research showing that dilauroylphosphatidylcholine (DLPC), a short-chain phospholipid which is partly soluble in water, can expel pre-adsorbed fibrinogen when adsorbing into fibrinogen monolayers from aqueous solution [39].

3.4. Mixing protocol II: fibrinogen added beneath a dipalmitoylphosphatidylcholine monolayer

The second mixing protocol introduces fibrinogen to the subphase beneath a pre-existing DPPC monolayer. DPPC

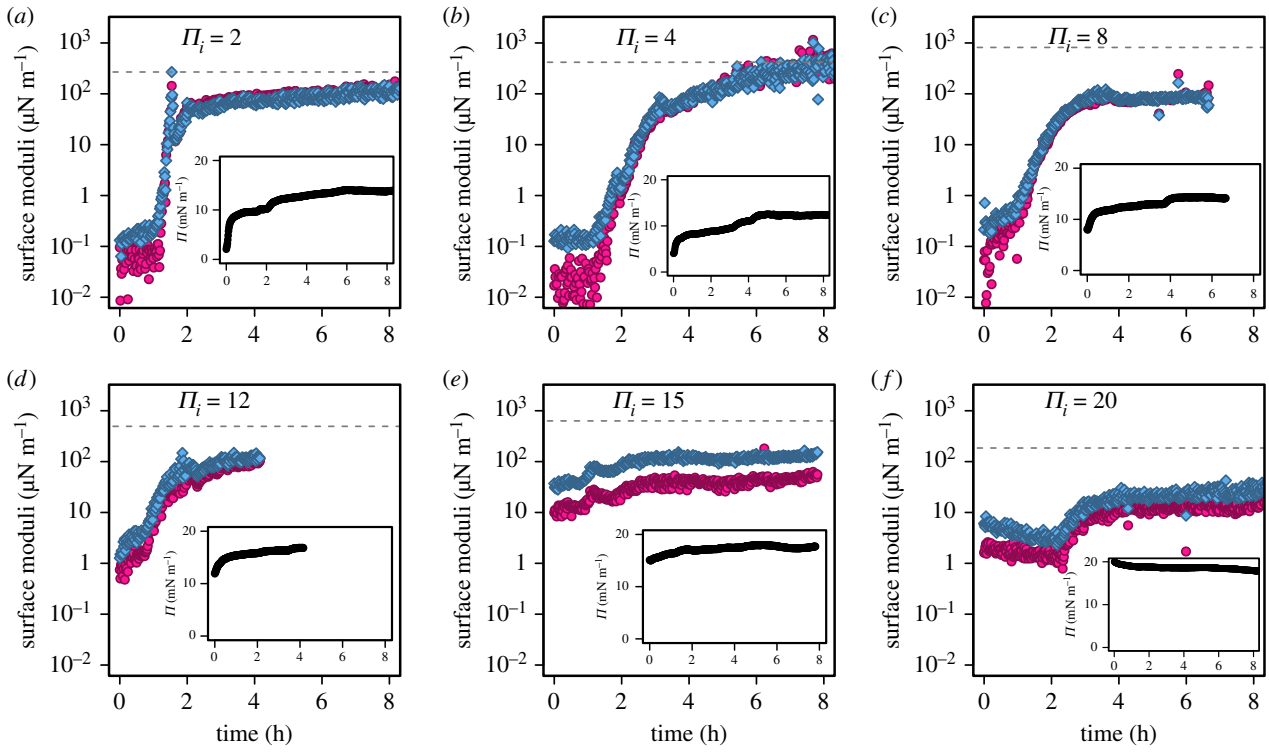

Figure 6. $G'_S(t)$ (pink circles) and $G''_S(t)$ (blue diamonds) when fibrinogen is injected into subphase below a DPPC monolayer at initial surface pressures (*a*) $\Pi_i = 2$ mN m^{-1}, (*b*) $\Pi_i = 4$ mN m^{-1}, (*c*) $\Pi_i = 8$ mN m^{-1}, (*d*) $\Pi_i = 12$ mN m^{-1}, (*e*) $\Pi_i = 15$ mN m^{-1}, (*f*) $\Pi_i = 20$ mN m^{-1}. Insets show $\Pi(t)$. Bulk subphase fibrinogen concentrations are in the range 0.003 mg ml^{-1} $< c <$ 0.006 mg ml^{-1}. Horizontal dashed lines indicate maximum measurable modulus.

is spread on PBS and compressed to initial surface pressure, Π_i. After a 30 min equilibration time, 0.5 ml of fibrinogen solution is injected into the subphase, and Π, surface rheology and monolayer morphology are subsequently measured as the interface evolves. A range of Π_i are investigated, from 2 to 20 mN m^{-1}, encompassing both fully LE and fully LC DPPC monolayers. The overall subphase concentration is in the range 0.003 mg ml^{-1} $< c <$ 0.006 mg ml^{-1}.

Figure 6 shows typical $G'_S(t)$ and $G''_S(t)$ curves following fibrinogen injection for the full range of Π_i. We first consider $\Pi(t)$, shown in the insets. In all but the experiment at $\Pi_i = 20$ mN m^{-1}, Π rises immediately following fibrinogen addition, without any induction period, indicating rapid monolayer penetration. This is consistent with studies of DPPC monolayer penetration by lysozyme [52]. The initial rise is steepest at lower Π_i and becomes more gradual with increasing Π_i. For $\Pi_i = 20$ mN m^{-1}, however, $\Pi(t)$ decreases slowly over approximately 8 h, likely due to subphase evaporation altering the buoyancy of the Wilhelmy plate. Presumably, evaporation also occurs in experiments at other Π_i, but, its effect is overshadowed by fibrinogen penetrating the monolayer. The evolution of G'_S and G''_S at $\Pi_i = 20$ mN m^{-1} reveal that fibrinogen does interact with the high Π DPPC at the interface.

The interfacial moduli, G'_S and G''_S, do not show an immediate rise at $t = 0$. The interface initially exhibits a viscous-dominated shear response characteristic of DPPC. After an onset time, during which Π increases, G'_S and G''_S rise and ultimately approach long-time plateaux. For $\Pi_i \lesssim$ 12 mN m^{-1} these plateaux are approximately 10^2 μN m^{-1} and $G'_S \sim G''_S$, indicating a mixed visco-elastic response. When fibrinogen adsorbs to fully LC DPPC monolayers ($\Pi_i \gtrsim$ 12 mN m^{-1}), the mixed monolayer does not become so stiff, and G''_S remains larger than G'_S, characteristic of a more DPPC-like, viscous-dominated shear response. Subphase fibrinogen concentration c is found to have little effect on end-state G'_S, G''_S or Π and so we focus on Π_i. The effect of c on the dynamics of monolayer penetration is explored in the electronic supplementary material.

One might anticipate that DPPC monolayers at Π_i greater than the spreading pressure of fibrinogen, Π_0, at a given subphase concentration, c, will effectively exclude fibrinogen. However, the data in figure 6 do not support this hypothesis. The spreading pressure of fibrinogen without DPPC (figure 2*b*) is in the range 7 to 10 mN m^{-1} for the concentrations employed here. That both Π and the interfacial moduli increase following fibrinogen injection, even for $\Pi_i > \Pi_0$ reveals non-trivial interactions between DPPC and fibrinogen.

Additional insight into monolayer evolution appears when G'_S is plotted versus Π rather than time (figure 7*a*). Π rises immediately on fibrinogen addition, but without any concurrent change in G'_S, as indicated by the flat regions on the left of each data series. As monolayer penetration proceeds, G'_S and G''_S increase by several orders of magnitude while Π remains fairly constant. Finally, Π continues to increase, while G'_S and G''_S approach their plateaux. The surface pressure at which the sharp rise in G'_S and G''_S occurs increases with Π_i, shifting the data to the right. This behaviour contrasts with fibrinogen absorption in the absence of DPPC (figure 3*c*), where G'_S and G''_S rise well before any change in Π is measured.

The simplest model interaction between fibrinogen and DPPC at the interface is one of area exclusion, neglecting interspecies attractions or repulsions. The surface number density of DPPC, Γ_{DPPC}, can be determined as a function of Π from the DPPC isotherm (figure 4*a*). Before fibrinogen injection, the entire interface is occupied by DPPC at surface pressure Π_i, corresponding to a molecular density $\Gamma_{\mathrm{DPPC}}(\Pi_i)$.

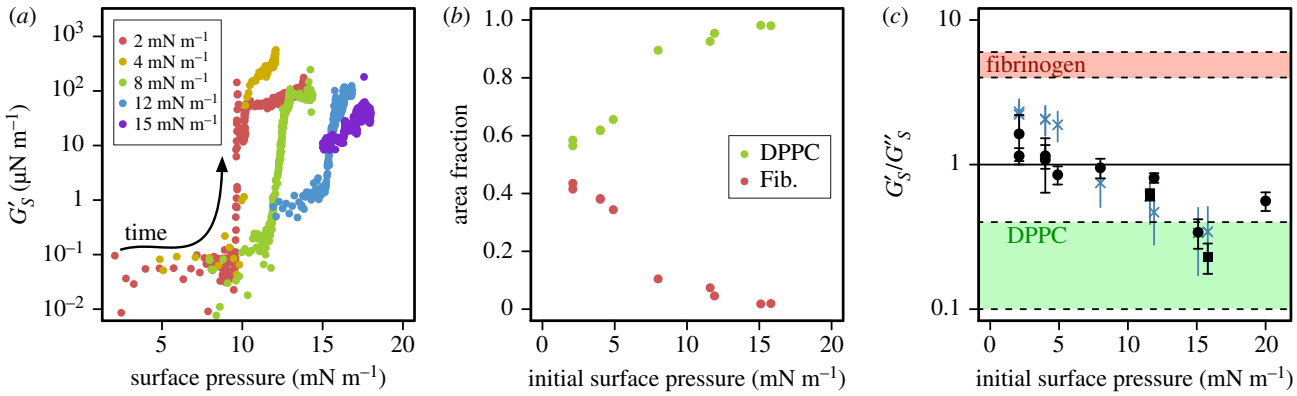

Figure 7. (*a*) $G'_S(\Pi)$ during monolayer penetration at Π_i indicated in legend with subphase fibrinogen concentrations in range 0.003 mg ml$^{-1} < c <$ 0.006 mg ml^{-1}. Time proceeds in direction of arrow. (*b*) End-state ϕ_{DPPC} (green) and ϕ_{Fib} (red) predicted by the excluded area model. (*c*) Experimentally measured averages (solid black points) and excluded area model predictions (blue crosses) of end-state ratio G'_S/G''_S as a function of Π_i. For rheological measurements, error bars represent standard deviation in time-average. For model predictions, error bars span range from minimum to maximum prediction based on single species rheology. Circles represent subphase fibrinogen concentrations in range 0.003 mg ml$^{-1} < c <$ 0.006 mg ml^{-1}, squares are $c \approx 1$ mg ml^{-1}.

As fibrinogen enters the interface, it reduces the area available to DPPC. As DPPC is insoluble in the subphase, the number of DPPC molecules on the interface is conserved, and their density is increased. Correspondingly, under the non-interacting, area exclusion approximation, Π increases following the DPPC isotherm. Comparing the initial and final surface pressures, Π_i and Π_f, in a monolayer penetration experiment, gives an estimate for the increase in Γ_{DPPC} and thus the end-state interfacial area fractions occupied by both DPPC and fibrinogen:

$$\phi_{DPPC} = \frac{\Gamma_{DPPC}(\Pi_i)}{\Gamma_{DPPC}(\Pi_f)} \tag{3.2}$$

and

$$\phi_{Fib} = 1 - \phi_{DPPC}. \tag{3.3}$$

For $\Pi_i \gtrsim 10$ mN m^{-1}, where DPPC starts in the fully LC state, (3.3) predicts that less than 10% of the end-state mixed monolayer is occupied by fibrinogen (figure 7*b*). This contrasts with lower Π_i monolayers with significant LE regions where fibrinogen is predicted to comprise up to approximately 40% of the end-state area. The predicted ϕ_{Fib} drops significantly across the Π_i range corresponding to LE–LC coexistence.

Armed with these predictions, we can consider the crossover from mixed viscoelastic behaviour to a viscous-dominated response as Π_i is increased. We characterize the monolayer using the ratio G'_S/G''_S, which is $\gg 1$ for elastic systems, $\ll 1$ for viscous systems and approximately 1 when the response is mixed. Pure fibrinogen typically shows elastic dominated behaviour (figure 3) with G'_S/G''_S between 4 and 6. Conversely, pure DPPC is viscous-dominated with G'_S/G''_S between 0.1 and 0.4. The end-state ratios G'_S/G''_S measured in monolayer penetration experiments are shown as a function of Π_i as black points in figure 7*c*, with single-component monolayer ranges indicated by shading. This quantitative assessment echoes the qualitative statements made previously: as Π_i increases, the end-state rheology crosses over from mixed viscoelastic behaviour ($G'_S/G''_S \sim 1$) to a viscous-dominated response $G'_S/G''_S < 1$. At high Π_i, this ratio approaches the values measured in pure DPPC, further supporting the claim that the monolayer retains a primarily DPPC-like character. For low Π_i, G'_S/G''_S indicates mixed-to-elastic behaviour, although the degree of elastic-dominance does not approach the values typical of pure fibrinogen. This indicates that DPPC still plays a significant role in determining the shear response of the mixed monolayer.

Using ϕ_{DPPC} and ϕ_{Fib} calculated from Π_i and Π_f, predictions of G'_S/G''_S are made using an area-weighted linear combination of the typical ratios measured in the single component monolayers:

$$\frac{G'_S}{G''_S} = \phi_{DPPC}\frac{G'_S}{G''_S}\bigg|_{DPPC} + \phi_{Fib}\frac{G'_S}{G''_S}\bigg|_{Fib}. \tag{3.4}$$

These are shown in blue in figure 7*c*. The crosses mark predictions made using the average pure monolayer ratios, and the error bars extend to the minimum and maximum predictions. However crude, this reductionist model captures the observed behaviour remarkably well, especially for $\Pi_i \gtrsim 8$ mN m^{-1}. At lower Π_i the predicted G'_S/G''_S is higher than measured in experiment, closer to that of pure fibrinogen. This suggests that, in this region, the excluded area model overestimates ϕ_{Fib}, or that interactions between the two species become more important when neither occupies an overwhelming majority of the interfacial area.

For $\Pi_i \lesssim 10$ mN m^{-1}, the monolayer can be directly observed using fluorescence microscopy during the penetration process, supplementing the insight gained from the excluded area model. For higher Π_i, the initial monolayer is entirely LC DPPC which excludes the fluorophore, and so morphology cannot be monitored.

Figure 8 shows a typical series of micrographs illustrating the effect of fibrinogen on a DPPC monolayer at $\Pi_i = 4$ mN m^{-1}. The initial monolayer has a low coverage of LC domains as shown in (*a*). After injection, the subphase fibrinogen concentration is $c \approx 0.005$ mg ml^{-1}, causing rapid increases in the interfacial moduli and Π. LC domains grow immediately, with a remarkable increase in their surface coverage occurring in the first 6 min (figure 8*a*,*b*). Domains initially grow with the spiral arms characteristic of pure DPPC LC domains [32,53,54], but these relax as the monolayer ages, becoming increasingly circular (figure 8*c*) while surface coverage continues to increase. After 2 h, the domains begin to deform against one another, creating a foam-like morphology (figure 8*d*), even though no change in Π is measured after 1 h.

These micrographs suggest a plausible mechanism for the evolution of G'_S and G''_S of lower Π_i experiments. Initially,

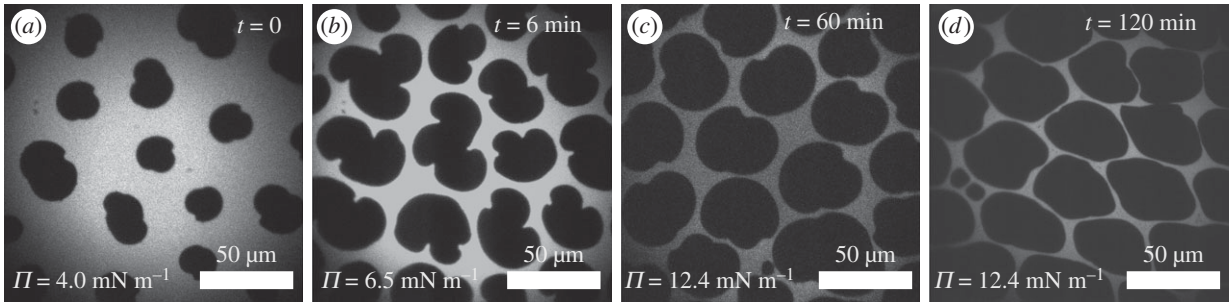

Figure 8. Fluorescence micrographs showing time evolution of DPPC monolayer morphology when fibrinogen is added to the subphase at $c \approx 0.005$ mg ml^{-1}. Initial surface pressure is $\Pi = 4$ mN m^{-1}. Brightness and contrast altered to mitigate the effects of photobleaching.

fibrinogen molecules adsorb at the interface, driving DPPC molecules into LC domains, causing their growth, and increasing Π. During this coexistence G'_S and G''_S are largely dominated by the continuous, LE phase and so do not change much. Once domains come into contact, rheology changes qualitatively. We speculate that the contact point corresponds to the sharp rise in G'_S and G''_S (figure 7*a*) as the contact between adjacent domains creates an increasingly 'jammed' system of stiff, condensed domains. Under this interpretation, the later, slower stiffening is attributed to a slow increase in jamming as domains deform against one another, resulting in the foam-like structures in figure 8*d*.

The fact that interfacial morphology continues to evolve despite no measurable change in Π between figure 8*c*,*d* suggests that Π alone cannot be used to characterize monolayer penetration. Exactly where fibrinogen incorporates into the DPPC monolayer is not clear from the micrographs. Small dark features that are not observed in pure DPPC monolayers appear within the LE phase (figure 8*d*) and seem clearly associated with fibrinogen. LC DPPC does not entirely exclude fibrinogen, however. Even fully LC DPPC monolayers with $\Pi_i > 10$ mN m^{-1} show a steady increase in $\Pi(t)$ and their interfacial moduli, which indicates fibrinogen adsorption. The smaller extent of this increase suggests that far less fibrinogen is adsorbed under these conditions, as reflected in the excluded area predictions of ϕ_{Fib}. It is plausible that fibrinogen can more easily penetrate disordered LE DPPC than ordered LC domains and we, therefore, propose that most fibrinogen adsorption initially occurs in the LE regions.

3.5. Lung surfactant under physiological conditions

Having characterized the consequences of mixing fibrinogen with DPPC at the aqueous–air interface under laboratory conditions, it is prudent to highlight and discuss the differences between our model experiments and the physiological conditions in the lung. Although the literature abounds with LS-inspired studies performed at room temperature [32,49,50,55–64] and/or using a single lipid [30,32,50,55,59,61–63] or simplified two- or three-component mixtures [7,30,49,56–58,60,65–68], LS operates at body temperature, 37°C, and consists of a mixture of DPPC with various additional saturated and unsaturated phospholipids, cholesterol, neutral lipids and four surfactant proteins [1,8]. Furthermore, physiological LS exists at surface pressures in the range 50 mN m^{-1} $\lesssim \Pi \lesssim$ 70 mN m^{-1} [1,2,6], significantly higher than those considered in our research, and is adsorbed at curved, rather than planar, interfaces.

In pure DPPC, LE–LC coexistence occurs at higher surface pressure as temperature is increased, and is suppressed entirely for $T \gtrsim 41$°C, beyond which LE DPPC exists at all Π [44,46–48]. Hermans & Vermant [44] demonstrated the importance of temperature in determining the rheological response of a DPPC monolayer, although viscous-dominated behaviour is observed up to 45°C and $\Pi = 45$ mN m^{-1}. As our data suggest that fibrinogen preferentially penetrates disordered LE DPPC, we speculate that increasing temperature towards the physiological regime would allow more fibrinogen to penetrate a DPPC monolayer at a given initial Π_i due to a decrease in the interfacial area occupied by LC DPPC domains at elevated temperature. That is, the 'capacity' for the DPPC monolayer to accommodate fibrinogen may increase with temperature due to persistence of disorder up to higher surface pressures.

But what of true LS? Up to 25% of native LS is unsaturated phospholipid, which does not incorporate into LC domains [1,69], and so significant disordered fluid regions exist at all Π below monolayer collapse. The coexistence of ordered and disordered regions is observed in LS at the high surface pressures and elevated temperatures of the physiological environment [70–73]. So, while we have focused on pure DPPC at room temperature and moderate Π around LC–LE coexistence, our model monolayers show morphological similarities with true LS under physiological conditions. Our data suggest that it is the distinction between LC and LE regions (i.e. ordered and disordered regions) that most significantly impacts the penetrability of the DPPC monolayer, rather than its surface pressure. It is, of course, unlikely that fibrinogen interacts with high Π, high-temperature LS in exactly the manner we have described, but it is plausible that similar physical effects may be observed. This remains an open and active avenue of investigation.

Finally, recent research has shown that the morphology of LC regions in a monolayer of Survanta, an animal-derived therapeutic pulmonary surfactant, depends upon the curvature of its underlying interface [73]. LC domains become connected as the interfacial radius of curvature is decreased to length-scales comparable to that of an alveolus, likely having significant impact on the interfacial rheology. As our description of interfacial stiffening due to the fibrinogen–DPPC interaction is based on monolayer morphology, it is likely that monolayer penetration will proceed differently on a highly curved interface.

Therefore, although the conditions of our experiments differ from those of physiological LS, we propose that the processes we have observed and phenomena we have measured in a simple, one-component phospholipid monolayer will have analogous processes in more physiologically relevant systems. Lung surfactant is a complex material, and we believe that our findings can serve as a foundation onto which complexity may be built, ultimately leading to a

physico-chemical understanding of the interaction of fibrinogen with LS under physiological conditions.

4. Conclusion

Four sets of experiments—two combining fibrinogen and DPPC via distinct protocols and two investigating the single species monolayers—reveal the effect of fibrinogen on the DPPC monolayer to be far from simple. Combining measurements of surface pressure, interfacial rheology, and monolayer morphology allows us to draw a number of conclusions, the overarching theme of which is that the behaviour of the mixed DPPC–fibrinogen system depends strongly on its preparation. It is established that the pressure–area isotherms of mixed DPPC–fibrinogen monolayers are influenced by surface initial conditions [74], and here we extend this result to encompass morphology and rheology.

In the absence of DPPC, fibrinogen adsorbing from bulk solution behaves in a manner as has been reported for protein adsorption in other systems [41,42]. As surface concentration increases, Π rises, eventually reaching a plateau as equilibrium is established. Adsorption proceeds more quickly and Π rises to a higher plateau as concentration is increased. Above an onset concentration, the fibrinogen monolayer exhibits a strongly elastic shear response. This contrasts with DPPC monolayers, which are viscous dominated.

DPPC is ineffective at displacing adsorbed fibrinogen monolayers, even when fibrinogen is so dilute that it causes no measurable change in Π or interfacial rheology. Instead, fluorescence imaging shows that new interfacial structures are formed following compression and decompression. This contrasts with the inverted order of operations, when fibrinogen penetrates pre-existing DPPC monolayers. The micrographs in figures 5 and 8 show that qualitatively different domain structures are formed, presumably reflecting differences in the molecular compositions of the mixed monolayers. This in itself is a remarkable result—the complexation of DPPC and fibrinogen is so strongly dependent upon preparation protocol that distinct interfacial mesostructures are apparent when the order of mixing is inverted.

These differences are reflected in the interfacial shear rheology. Without fibrinogen, the response of a DPPC monolayer is viscous-dominated. This contrasts with pure fibrinogen, which exhibits strongly elastic behaviour (figure 3). The properties of mixed DPPC-fibrinogen monolayers vary from elastic-dominated (fibrinogen-like) to viscous-dominated (DPPC-like) depending on their preparation. The most elastic behaviour is found when DPPC is spread onto preadsorbed fibrinogen (figure 4). When fibrinogen penetrates a pre-existing DPPC monolayer, the response depends on the initial surface pressure. A mixed viscoelastic end-state is evident at low Π_i, neither entirely fibrinogen-like nor entirely DPPC-like. Increasing Π_i gives increasingly viscous-dominated end-states, which retain some of the characteristics of pure DPPC.

The condensed DPPC monolayer at high Π_i is more effective at excluding fibrinogen than it is at low Π_i, but LC DPPC does not entirely block fibrinogen from the interface. A simple excluded area model of monolayer penetration predicts that fibrinogen occupies less than 10% of the area in the end-state mixed monolayer when DPPC is initially in its fully LC state. This model makes remarkably good predictions of end-state rheology in this regime. At lower Π_i in which LE DPPC predominates, our model suggests that fibrinogen may occupy up to 40% of the interfacial area.

The timescales characterizing the rise in Π and the interfacial moduli during fibrinogen adsorption can differ significantly. Without DPPC, G'_S and G''_S increase more quickly than Π and much of the interfacial stiffening occurs at $\Pi = 0\,\mathrm{mN\,m^{-1}}$. Conversely, when DPPC is initially present, Π increases before G'_S and G''_S. A corollary of this finding is that measurements of surface pressure are insufficient to fully characterize monolayer penetration. An apparent plateau in Π does not necessarily indicate equilibrium, as the interfacial viscoelastic moduli and monolayer morphology may continue to evolve at constant Π.

Under certain circumstances, fibrinogen can significantly impact the shear rheology of DPPC monolayers. *In vivo*, a change in behaviour from viscous- to elastic-dominated could have dramatic implications, potentially inhibiting the respreading of LS on alveolar expansion or hindering interfacial transport, preventing the expulsion of foreign material from the lung. Our model studies provide new insight into the mechanical and morphological aspects of the interaction between surface active proteins and phospholipids, and may serve as a foundation for a deeper understanding of LS inactivation.

Data accessibility. Experimental data are available online at http://doi.org/10.6084/m9.figshare.5655805.v1 [75].

Authors' contributions. I.W. designed research, performed experiments, analysed data and drafted the manuscript. T.M.S. conceived of and coordinated the study and helped draft the manuscript. Both the authors gave their final approval for publication.

Competing interests. The authors declare no conflict of interests.

Funding. Research reported in this publication was supported by the National Heart, Lung, and Blood Institute of the National Institutes of Health under grant numbers R01HL135065 and R01HL51177. The content is solely the responsibility of the authors and does not necessarily represent the official views of the National Institutes of Health.

Acknowledgements. The authors express their gratitude to Joseph Zasadzinski, Amit Sachan, Sourav Barman, Nick Cadirov and Arash Nowbahar for enlightening discussion and to Harishankar Manikantan for critical reading of the manuscript.

References

1. Parra E, Pérez-Gil J. 2015 Composition, structure and mechanical properties define performance of pulmonary surfactant membranes and films. *Chem. Phys. Lipids* **185**, 153–175. (doi:10.1016/j.chemphyslip.2014.09.002)
2. Zasadzinski J, Stenger P, Shieh I, Dhar P. 2010 Overcoming rapid inactivation of lung surfactant: analogies between competitive adsorption and colloid stability. *BBA-Biomembranes* **1798**, 801–828. (doi:10.1016/j.bbamem.2009.12.010)
3. Pérez-Gil J. 2008 Structure of pulmonary surfactant membranes and films: the role of proteins and lipid–protein interactions. *BBA-Biomembranes* **1778**, 1676–1695. (doi:10.1016/j.bbamem.2008.05.003)

4. Clements J, Avery M. 1998 Lung surfactant and neonatal respiratory distress syndrome. *Am. J. Resp. Crit. Care* **157**, S59–S66. (doi:10.1164/ajrccm.157.4.nhlb1-1)
5. Daniels C, Orgeig S. 2003 Pulmonary surfactant: the key to the evolution of air breathing. *News Physiol. Sci.* **18**, 151–157.
6. Schürch S, Goerke J, Clements J. 1976 Direct determination of surface tension in the lung. *Proc. Natl Acad. Sci. USA* **73**, 4698–4702. (doi:10.1073/pnas.73.12.4698)
7. Bringezu F, Ding J, Brezesinski G, Zasadzinski J. 2001 Changes in model lung surfactant monolayers induced by palmitic acid. *Langmuir* **17**, 4641–4648. (doi:10.1021/la0103158)
8. Zuo Y, Veldhuizen R, Neumann A, Petersen N, Possmayer F. 2008 Current perspectives in pulmonary surfactant—inhibition, enhancement and evaluation. *BBA-Biomembranes* **1778**, 1947–1977. (doi:10.1016/j.bbamem.2008.03.021)
9. Pison U, Herold R, Schürch S. 1996 The pulmonary surfactant system: biological functions, components, physicochemical properties and alterations during lung disease. *Colloid Surface A* **114**, 165–184. (doi:10.1016/0927-7757(96)03572-8)
10. Ware L, Matthay M. 2000 The acute respiratory distress syndrome. *New Engl. J. Med.* **342**, 1334–1349. (doi:10.1056/NEJM200005043421806)
11. Avery M. 2000 Surfactant deficiency in hyaline membrane disease: the story of discovery. *Am. J. Resp. Crit. Care* **161**, 1074–1075. (doi:10.1164/ajrccm.161.4.16142)
12. Spragg R *et al.* 2004 Effect of recombinant surfactant protein C-based surfactant on the acute respiratory distress syndrome. *New Engl. J. Med.* **351**, 884–892. (doi:10.1056/NEJMoa033181)
13. McIntyre R, Pulido E, Bensard D, Shames B, Abraham E. 2000 Thirty years of clinical trials in acute respiratory distress syndrome. *Crit. Care Med.* **28**, 3314–3331. (doi:10.1097/00003246-200009000-00034)
14. Holm B, Wang Z, Notter R. 1999 Multiple mechanisms of lung surfactant inhibition. *Pediatr. Res.* **46**, 85–93. (doi:10.1203/00006450-199907000-00015)
15. Warriner H, Ding J, Waring A, Zasadzinski J. 2002 A concentration-dependent mechanism by which serum albumin inactivates replacement lung surfactants. *Biophys. J.* **82**, 835–842. (doi:10.1016/S0006-3495(02)75445-3)
16. Nakos G, Kitsiouli E, Tsangaris I, Lekka M. 1998 Bronchoalveolar lavage fluid characteristics of early intermediate and late phases of ARDS. Alterations in leukocytes, proteins, PAF and surfactant components. *Intensive Care Med.* **24**, 296–303. (doi:10.1007/s001340050571)
17. Günther A, Ruppert C, Schmidt R, Markart P, Grimminger F, Walmrath D, Seeger W. 2001 Surfactant alteration and replacement in acute respiratory distress syndrome. *Respir. Res.* **2**, 353–364. (doi:10.1186/rr86)
18. Seeger W, Stöhr G, Wolf H, Neuhof H. 1985 Alteration of surfactant function due to protein leakage: special interaction with fibrin monomer. *J. Appl. Physiol.* **58**, 326–338. (doi:10.1152/jappl.1985.58.2.326)
19. Seeger W, Gunther A, Thede C. 1992 Differential sensitivity to fibrinogen inhibition of SP-C- vs. SP-B-based surfactants. *Am. J. Physiol.* **261**, L286–L291. (doi:10.1152/ajplung.1992.262.3.L286)
20. Fuchimukai T, Fujiwara T, Takahashi A, Enhorning G. 1987 Artificial pulmonary surfactant inhibited by proteins. *J. Appl. Physiol.* **62**, 429–437. (doi:10.1152/jappl.1987.62.2.429)
21. Holm B, Notter R, Finkelstein J. 1985 Surface property changes from interactions of albumin with natural lung surfactant and extracted lung lipids. *Chem. Phys. Lipids* **38**, 287–298. (doi:10.1016/0009-3084(85)90022-2)
22. Holm B, Notter R. 1987 Effects of hemoglobin and cell membrane lipids on pulmonary surfactant activity. *J. Appl. Physiol.* **63**, 1434–1442. (doi:10.1152/jappl.1987.63.4.1434)
23. Gregory T *et al.* 1991 Surfactant chemical composition and biophysical activity in acute respiratory distress syndrome. *J. Clin. Invest.* **88**, 1976–1981. (doi:10.1172/JCI115523)
24. Hernández E, Phang TL, Wen X, Franses E. 2002 Adsorption and direct probing of fibrinogen and sodium myristate at the air/water interface. *J. Colloid Interf. Sci.* **250**, 271–280. (doi:10.1006/jcis.2002.8360)
25. Hernández E, Franses E. 2003 Adsorption and surface tension of fibrinogen at the air/water interface. *Colloid Surface A* **214**, 249–262. (doi:10.1016/S0927-7757(02)00403-X)
26. Hassan N, Maldonado-Valderrama J, Gunning A, Morris V, Ruso J. 2011 Surface characterization and AFM imaging of mixed fibrinogen-surfactant films. *J. Phys. Chem. B* **115**, 6304–6311. (doi:10.1021/jp200835j)
27. Bratek-Skicki A, Zeliszewska P, Ruso J. 2016 Fibrinogen: a journey into biotechnology. *Soft Matter* **12**, 8639–8653. (doi:10.1039/C6SM01895E)
28. Zell Z, Mansard V, Wright J, Kim K, Choi S, Squires T. 2016 Linear and nonlinear microrheometry of small samples and interfaces using microfabricated probes. *J. Rheol.* **60**, 141–159. (doi:10.1122/1.4937931)
29. Lösche M, Möhwald H. 1984 Fluorescence microscope to observe dynamical processes in monomolecular layers at the air/water interface. *Rev. Sci. Instrum.* **55**, 1968–1972. (doi:10.1063/1.1137688)
30. Gaub HE, Moy VT, McConnell HM. 1986 Reversible formation of plastic two-dimensional lipid crystals. *J. Phys. Chem.* **90**, 1721–1725. (doi:10.1021/j100399a051)
31. Zell ZA, Nowbahar A, Mansard V, Leal LG, Deshmukh SS, Mecca JM, Tucker CJ, Squires TM. 2014 Surface shear inviscidity of soluble surfactants. *Proc. Natl Acad. Sci. USA* **111**, 3677–3682. (doi:10.1073/pnas.1315991111)
32. Kim K, Choi S, Zasadzinski J, Squires T. 2011 Interfacial microrheology of DPPC monolayers at the air–water interface. *Soft Matter* **7**, 7782–7789. (doi:10.1039/C1SM05383C)
33. Choi S, Steltenkamp S, Zasadzinski J, Squires T. 2011 Active microrheology and simultaneous visualization of sheared phospholipid monolayers. *Nat. Commun.* **2**, 312. (doi:10.1038/ncomms1321)
34. Hughes B, Pailthorpe B, White L. 1981 The translational and rotational drag on a cylinder moving in a membrane. *J. Fluid Mech.* **110**, 349–372. (doi:10.1017/S0022112081000785)
35. Krägel J, Derkatch S, Miller R. 2008 Interfacial shear rheology of protein–surfactant layers. *Adv. Colloid Interface* **144**, 38–53. (doi:10.1016/j.cis.2008.08.010)
36. Roberts S, Kellaway I, Taylor K, Warburton B, Peters K. 2005 Combined surface pressure–interfacial shear rheology study of the effect of pH on the adsorption of proteins at the air–water interface. *Langmuir* **21**, 7342–7348. (doi:10.1021/la050272l)
37. Ariola F, Krishnan A, Vogler E. 2006 Interfacial rheology of blood proteins adsorbed to the aqueous-buffer/air interface. *Biomaterials* **27**, 3404–3412. (doi:10.1016/j.biomaterials.2006.02.005)
38. Hassan N, Maldonado-Valderrama J, Gunning A, Morris V, Ruso J. 2011 Investigating the effect of an arterial hypertension drug on the structural properties of plasma protein. *Colloid Surface B* **87**, 489–497. (doi:10.1016/j.colsurfb.2011.06.015)
39. Phang T, McClellan S, Franses E. 2005 Displacement of fibrinogen from the air/aqueous interface by dilauroylphosphatidylcholine lipid. *Langmuir* **21**, 10 140–10 147. (doi:10.1021/la0504412)
40. Vörös J. 2004 The density and refractive index of adsorbing protein layers. *Biophys. J.* **87**, 553–561. (doi:10.1529/biophysj.103.030072)
41. Ybert C, di Meglio JM. 1998 Study of protein adsorption by dynamic surface tension measurements: diffusive regime. *Langmuir* **14**, 471–475. (doi:10.1021/la970999c)
42. Miller R, Fainerman V, Aksenenko E, Leser M, Michel M. 2004 Dynamic surface tension and adsorption kinetics of beta-casein at the solution/air interface. *Langmuir* **20**, 771–777. (doi:10.1021/la030332s)
43. Kaganer V, Möhwald H, Dutta P. 1999 Structure and phase transitions in Langmuir monolayers. *Rev. Mod. Phys.* **71**, 779–819. (doi:10.1103/RevModPhys.71.779)
44. Hermans E, Vermant J. 2014 Interfacial shear rheology of DPPC under physiologically relevant conditions. *Soft Matter* **10**, 175–186. (doi:10.1039/C3SM52091A)
45. Weis R. 1991 Fluorescence microscopy of phospholipid monolayer phase transitions. *Chem. Phys. Lipids* **57**, 227–239. (doi:10.1016/0009-3084(91)90078-P)
46. Rice DK, Cadenhead DA, Lewis RNAH, McElhaney RN. 1987 A comparative monomolecular film study of a straight-chain phosphatidylcholine (dipalmitoylphosphatidylcholine) with three isobranched-chain phosphatidylcholines (diisoheptadecanoylphosphatidylcholine, diisooctadecanoylphosphatidylcholine, and diisoeicosanoylphosphatidylcholine). *Biochemistry* **26**, 3205–3210. (doi:10.1021/bi00385a040)

47. Toimil P, Prieto G, Mi?ones J, Sarmiento F. 2010 A comparative study of F-DPPC/DPPC mixed monolayers. Influence of subphase temperature on F-DPPC and DPPC monolayers. *Phys. Chem. Chem. Phys.* **12**, 13 323–13 332. (doi:10.1039/c0cp00506a)
48. Shieh IC, Zasadzinski JA. 2015 Visualizing monolayers with a water-soluble fluorophore to quantify adsorption, desorption, and the double layer. *Proc. Natl Acad. Sci. USA* **112**, E826–E835. (doi:10.1073/pnas.1419033112)
49. Sachan AK, Choi SQ, Kim KH, Tang Q, Hwang L, Lee KYC, Squires TM, Zasadzinski JA. 2017 Interfacial rheology of coexisting solid and fluid monolayers. *Soft Matter* **13**, 1481–1492. (doi:10.1039/C6SM02797K)
50. Kuo RR, Chang CH, Yang YM, Maa JR. 2003 Induced removal of dipalmitoyl phosphatidylcholine by the exclusion of fibrinogen from compressed monolayers at air/liquid interfaces. *J. Colloid Interface Sci.* **257**, 108–115. (doi:10.1016/S0021-9797(02)00024-3)
51. Kobayashi H, Sasaki M, Ohsawa N, Yasuda K, Kotani M. 2007 Fluorescence and its density-dependent quenching of a sub-monolayer film of methylene blue prepared by dip coating. *J. Phys. Chem. C* **111**, 268–271. (doi:10.1021/jp064558q)
52. Sundaram S, Stebe K. 1997 Dynamic penetration of an insoluble monolayer by a soluble surfactant: theory and experiment. *Langmuir* **13**, 1729–1736. (doi:10.1021/la9609938)
53. Moy V, Keller D, Gaub H, McConnell H. 1986 Long-range molecular orientational order in monolayer solid domains of phospholipid. *J. Phys. Chem.* **90**, 3198–3202. (doi:10.1021/j100405a030)
54. McConlogue C, Malamud D, Vanderlick T. 1998 Interaction of DPPC monolayers with soluble surfactants: electrostatic effects of membrane perturbants. *BBA-Biomembranes* **1372**, 124–134. (doi:10.1016/S0005-2736(98)00052-2)
55. Borissevitch GP, Tabak M, Oliveira ON. 1996 Interaction of dipyridamole with lipids in mixed Langmuir monolayers. *Biochim. Biophys. Acta - Biomembr.* **1278**, 12–18. (doi:10.1016/0005-2736(95)00208-1)
56. Kim K, Choi S, Zell Z, Squires T, Zasadzinski J. 2013 Effect of cholesterol nanodomains on monolayer morphology and dynamics. *Proc. Natl Acad. Sci. USA* **110**, E3054–E3060. (doi:10.1073/pnas.1303304110)
57. Choi SQ, Kim K, Fellows CM, Cao KD, Lin B, Lee KYC, Squires TM, Zasadzinski JA. 2014 Influence of molecular coherence on surface viscosity. *Langmuir* **30**, 8829–8838. (doi:10.1021/la501615g)
58. Ding J, Warriner HE, Zasadzinski JA. 2002 Viscosity of two-dimensional suspensions. *Phys. Rev. Lett.* **88**, 168102. (doi:10.1103/PhysRevLett.88.168102)
59. Farnoud AM, Fiegel J. 2012 Low concentrations of negatively charged sub-micron particles alter the microstructure of DPPC at the air–water interface. *Colloids Surf. A: Physicochem. Eng. Aspects* **415**, 320–327. (doi:10.1016/j.colsurfa.2012.10.001)
60. Guzmán E, Liggieri L, Santini E, Ferrari M, Ravera F. 2012 DPPC-DOPC Langmuir monolayers modified by hydrophilic silica nanoparticles: phase behaviour, structure and rheology. *Colloids Surf. A: Physicochem. Eng. Aspects* **413**, 174–183. (doi:10.1016/j.colsurfa.2011.12.059)
61. McConlogue CW, Vanderlick TK. 1997 A close look at domain formation in DPPC monolayers. *Langmuir* **13**, 7158–7164. (doi:10.1021/la970898e)
62. Miñones Jr J, Dynarowicz-Łatka P, Miñones J, Rodriguez Patino JM, Iribarnegaray E. 2003 Orientational changes in dipalmitoyl phosphatidyl glycerol Langmuir monolayers. *J. Colloid Interface Sci.* **265**, 380–385. (doi:10.1016/S0021-9797(03)00479-X)
63. Orsi D, Guzmán E, Liggieri L, Ravera F, Ruta B, Chushkin Y, Rimoldi T, Cristofolini L. 2015 2D dynamical arrest transition in a mixed nanoparticle–phospholipid layer studied in real and momentum spaces. *Sci. Rep.* **5**, 1–14. (doi:10.1038/srep17930)
64. Ruano ML, Nag K, Worthman LA, Casals C, Pérez-Gil J, Keough KM. 1998 Differential partitioning of pulmonary surfactant protein SP-A into regions of monolayers of dipalmitoylphosphatidylcholine and dipalmitoylphosphatidylcholine/dipalmitoylphosphatidylglycerol. *Biophys. J.* **74**, 1101–1109. (doi:10.1016/S0006-3495(98)77828-2)
65. Chakraborty A, Hui E, Waring AJ, Dhar P. 2016 Combined effect of synthetic protein, Mini-B, and cholesterol on a model lung surfactant mixture at the air–water interface. *Biochim. Biophys. Acta (BBA) - Biomembr.* **1858**, 904–912. (doi:10.1016/j.bbamem.2016.01.008)
66. Lawrie GA, Gentle IR, Barnes GT. 2000 The structure of mixed monolayer films of DPPC and hexadecanol. *Colloids Surf. A: Physicochem. Eng. Aspects* **171**, 217–224. (doi:10.1016/S0927-7757(99)00539-7)
67. Lee KYC, Gopal A, von Nahmen A, Zasadzinski Ja, Majewski J, Smith GS, Howes PB, Kjær K. 2002 Influence of palmitic acid and hexadecanol on the phase transition temperature and molecular packing of dipalmitoylphosphatidyl-choline monolayers at the air–water interface. *J. Chem. Phys.* **116**, 774–783. (doi:10.1063/1.1420730)
68. Picardi MV, Cruz A, Orellana G, Pérez-Gil J. 2011 Phospholipid packing and hydration in pulmonary surfactant membranes and films as sensed by LAURDAN. *Biochim. Biophys. Acta - Biomembr.* **1808**, 696–705. (doi:10.1016/j.bbamem.2010.11.019)
69. Takamoto DY, Lipp MM, von Nahmen A, Lee KY, Waring AJ, Zasadzinski JA. 2001 Interaction of lung surfactant proteins with anionic phospholipids. *Biophys. J.* **81**, 153–169. (doi:10.1016/S0006-3495(01)75688-3)
70. Lipp MM, Lee KYC, Zasadzinski JA, Waring AJ. 1996 Phase and morphology changes in lipid monolayers induced by SP-B protein and its amino-terminal peptide. *Science* **273**, 1196–1199. (doi:10.1126/science.273.5279.1196)
71. BernardinoDeLaSerna J, Perez-Gil J, Simonsen AC, Bagatolli LA. 2004 Cholesterol rules: direct observation of the coexistence of two fluid phases in native pulmonary surfactant membranes at physiological temperatures. *J. Biol. Chem.* **279**, 40 715–40 722. (doi:10.1074/jbc.M404648200)
72. Bernardino De La Serna J, Orädd G, Bagatolli LA, Simonsen AC, Marsh D, Lindblom G, Perez-Gil J. 2009 Segregated phases in pulmonary surfactant membranes do not show coexistence of lipid populations with differentiated dynamic properties. *Biophys. J.* **97**, 1381–1389. (doi:10.1016/j.bpj.2009.06.040)
73. Sachan AK, Zasadzinski JA. 2017 Interfacial curvature effects on the monolayer morphology and dynamics of a clinical lung surfactant. *Proc. Natl Acad. Sci. USA* **115**, E134–E143. (doi:10.1073/pnas.1715830115)
74. Tabak SA, Notter RH. 1976 Effect of plasma proteins on the dynamic Π—a characteristics of saturated phospholipid films. *J. Colloid Interface Sci.* **59**, 293–300. (doi:10.1016/0021-9797(77)90011-X)
75. Williams I, Squires TM. 2018 Data from: Evolution and mechanics of mixed phospholipid fibrinogen monolayers. Figshare: (doi:10.6084/m9.figshare.5655805)